Catalysis Science & Technology

Accepted Manuscript

ROYAL SOCIETY OF CHEMISTRY

www.rsc.org/catalysis

Adsorption and Desulfurization Reaction Mechanism of Thiophene and its Hydrogenated Derivatives over NbC(001) and NbN(001): An ab-initio DFT Study

*Eugenio Furtado de Souza** [1], *Teodorico C. Ramalho*[2], *Carlos Alberto Chagas*[3], *Ricardo Bicca de Alencastro*[1].

1) Universidade Federal do Rio de Janeiro. Rio de Janeiro, Instituto de Química. Programa de PG em Química.

Laboratorio de Modelagem Molecular-LABMMOL

Av. Athos da Silveira Ramos No 149, CT, Bloco A, sala 609.

tel: (21) 2562-7132 - fax: (21) 2562-7132

Cidade Universitária, Ilha do Fundão, Rio de Janeiro-RJ, CEP 21941-909.

e-mail- eugeniofs@iq.ufrj.br (Eugenio F. de Souza) – bicca@iq.ufrj.br **(Ricardo Bicca de Alencastro)**

2) Universidade Federal do Rio de Janeiro, Núcleo de Catálise, Programa de Engenharia Química, COPPE. Av. Horácio Macedo, 2030 - Centro de Tecnologia - Bloco G - Sala G-115

Ilha do Fundão – CEP 21941-914 - Rio de Janeiro, RJ - Brasil - Caixa-postal: 68502

Telefone: (21) 25628304 - Ramal: 3575 - Fax: (21) 25628300

email - carlosalbertoeq@yahoo.com.br (Carlos A. das Chagas)

4) Universidade Federal de Lavras, Departamento de Química.

Universidade Federal de Lavras, UFLA.

Departamento de Química, Campus Universitário – UFLA – CEP 37200-000 - Lavras, MG - Brasil - Caixa-postal: 3037 -Tel: (35) 38291552 Fax: (35) 38291271

email- teo@dqi.ufla.br (Teodorico C. Ramalho)

*eugeniofs@iq.ufrj.br

ABSTRACT: Herein, we present periodic DFT-based calculations on the thiophene adsorption and reaction pathways over niobium carbide and nitride cubic face-centered (001) surfaces by considering both direct (DDS) and hydrogenating (HYD) routes for further desulfurization reactions and evaluate the implications for the mechanism of hydrodesulfurization (HDS). The theoretical studies were based on ultrasoft pseudopotentials and a plane-wave basis set, and were performed with the help of the Quantum-ESPRESSO package. To understand the role of both surfaces in the adsorption and desulfurization process various starting configurations for the adsorbed thiophene were tested and the energetically most stable were used in bond breaking studies. It was observed that thiophene adsorbs preferentially in a η-5 configuration by interacting with the nitride surface through its π-structure whereas on the carbide surface thiophene was found to prefer a tilted η-1 configuration. Based on nudged elastic band (NEB) studies, our results suggest that the ring hydrogenation does not necessarily lead to a preference for the HYD pathway of thiophene desulfurization. Furthermore, surface and electronic effects were also evaluated. We have found that in ideal conditions the niobium nitride surface should present better performance for the desulfurization of thiophene than the carbide surface.

KEYWORDS: Niobium carbide, niobium nitride, thiophene, desulfurization, HDS, DFT, catalysis.

1. INTRODUCTION

Environmental regulations on the amounts of organosulfur compounds in liquid fuels has become more rigorous over the past decades [1]. Consequently, an increasing number of research works address the chemistry and the processing of petroleum derivatives [1,2]. The combustion of the sulfur-rich compounds present in these derivatives consists principally of the SO_x species which are strong catalysts poisons and forms a dangerous class of air pollutants, which in turn may conduct to the formation of acid rain [2]. Among these compounds, aromatic heterocyclic molecules like thiophene (C_4H_4S) and its derivatives notably 4,6-dimethyldibenzothiophene (4,6-DMDBT) are the most refractory to desulfurization [3]. In heterogeneous catalysis, thiophene has long served as a model for experimental and theoretical studies on desulfurization processes which deals mainly with the fundamental factors that govern the substrate-adsorbate complex, such as the nature of the active site, initial adsorption geometry, diffusion on the surface and catalytic activity.

Among the desulfurization processes, hydrodesulfurization (HDS) is commonly used in almost all refinery plants around the world [1]. The HDS process is one in a broad class of processes known as "hydroprocessing", used in order to reduce the nitrogen, oxygen, aromatics and sulfur contents from petroleum feedstocks [4,5]. In the case of HDS, fuels are exposed in the presence of catalysts usually sulfided NiMo/Al2O_3 or CoMo/Al_2O_3 and hydrogen gas (H_2) to pressure (2-20 bar) and high temperatures (340-410°C) [6]. Despite their efficiency they generally result in a reduction of the octane number due to the saturation of olefins, thus leading to lesser quality fuels and high H_2 consumption [7]. Therefore, the increasingly stringent legislation and environmental restrictions associated with the ever-growing global use of fossil fuels make necessary further efforts in research and development of new active phases [8].

Accordingly, it is known that the transition metal carbides and nitrides (TMCNs) possess unique chemical and physical properties, attracting considerable attention in different areas of technological interest like for example heterogeneous catalysis [9]. This class of compounds is characterized by metal-metal, metal-nitrogen (nitride) and metal-carbon (carbide) bonds which ensure a substantial gain in physical and chemical stability, and also an unusual combination of characteristics of ceramics and metals such as high melting point, excellent electric and thermal conductivities and extreme hardness which make them good candidates for practical applications and fundamental studies [10]. For example, recently our group has described a new solid-state synthesis route of vanadium nitride along with theoretical studies on the properties of an identified key-intermediate and on the solid-state transformations involved in the synthesis mechanism [64,89]. Since the pioneering work of Levy and Boudart [9], who observed that tungsten carbide (WC) possesses special catalytic properties which qualitatively resemble those of noble metals (Pt, Pd and Rh), TMCNs have been considered promising active phases. Hydrogenation of CO [11,12] or benzene [13,14], conversion of *n*-butane [15], water gas shift [16], ammonia synthesis [17], hydrocarbon isomerization [18], hydrodenitrogenation [19] are examples of reaciotions catalyzed by TMCNs. TMCN also shows interesting HDS properties [8]. A considerable number of papers deal with the interaction of thiophene with metal nitrides [47,48], carbides [49-51], sulfides [8,30,51-53], transition metals [54,55,62,80], alloys [56-59] and oxides [60,61]. For example, it was reported by Tominaga and Nagai [63] that the adsorption of thiophene on clean β-Mo_2C(001) causes the simultaneous breaking of the S-C bonds, resulting in a strongly exothermic adsorption profile (-10.8 eV). Nevertheless, up this date the most studied TMCNs in catalytic applications contain molybdenum (Mo) and/or tungsten (W) atoms, and this fact opens new possibilities for further investigating different TMCNs.

In particular, niobium carbides (NbC) and nitrides (NbN) are catalytically active in numerous reactions. For example, HDS and HDN (nitrogen) activities of unsupported NbN were also evaluated for heavy vacuum gasoil at ~350°C [21], showing relatively less activity than the commercial the catalyst, $NiMo/Al_2O_3$, but presenting better HDN activity when compared to the same catalyst. On the other hand, it was observed that NbC has low activity in HDS reactions although high resistance to S-poisoning [22]. Schwartz *et.al.* investigated the activity of the supported bimetallic niobium oxycarbide system, $NbMoOC/Al_2O_3$, in three Mo/Nb ratios (1.2, 1.6, 2.0), concluding that this catalyst is outstandingly active in HDN reactions and presents excellent activity in HDS of 4,6-DMDBT, higher than that of the commercial sulfided catalyst and comparable to Mo_2C/Al_2O_3 [23]. Recently, Chagas and co-workers [24] investigated a new solid-state synthesis route of $NbN_{1-x}C_x$ phases as well as the activity of the products in HDS of dibenzothiophene, observing higher performances for their catalyst in comparison with the catalyst synthesized by the commonly used TPC methodology. Despite its interesting and promising range of applications, experimental and theoretical studies on surface properties, reaction mechanisms, and catalytic activity of niobium carbides and nitrides are still scarce.

In line with these issues, computer simulations based on the Density Functional Theory (DFT) have given a valuable contribution to the elucidation of the complex phenomena resulting from the interactions of sulfur-containing species and catalytic surfaces providing qualitative and even quantitative insights [29,43,62,74,82,86]. To the best of our knowledge, details of the adsorption of thiophene and other organosulfur compounds on NbC and NbN surfaces as well as its desulfurization mechanisms have not yet been theoretically investigated *via* DFT calculations. It is worth noting that the most important event during the desulfurization process is the S-C bond cleavage [30] but in many cases the mechanism is still not completely understood. Moreover, the effects of hydrogenation and S-C bond weakening/breaking in

organosulfur compounds are still matter of debate [29]. Consequently, fundamental understanding of these mechanisms together with a detailed study of the TMCN surface properties, necessary to the development of new active phases and to allow extensions to other TMCN, have motivated us to carry out a computational investigation on the aspects involved in thiophene adsorption, hydrogenation and desulfurization process over the NbC(001) and NbN(001) surfaces, which should also be useful in understanding this process in other systems. In order to shed light on these issues, electronic and structural properties of the thiophene/NbC(001) [Th/NbC(001)] and thiophene/NbN(001) [Th/NbN(001)] systems were evaluated by using plane-wave periodic density functional theory. Furthermore, the effects of thiophene hydrogenation were also studied and the possible mechanisms involved discussed. The (001) plane was firstly chosen due to the fact that it generate a non-polarized surface, defined by equal numbers of metal and non-metal atoms and, according to experimental and theoretical studies, it represents the energetically most stable cleavage plane [25-28]. A systematic study of the the catalytic properties of the low-index surfaces of niobium carbide/nitride, namely (110) and (111), over thiophene desulfurization are now underway and will be the target for future publications.

2. COMPUTATIONAL METHODOLOGY

All calculations were performed within the framework of the Density Functional Theory (DFT) using the plane-wave pseudopotential total-energy method and employing the PWSCF computational code as implemented in the Quantum-ESPRESSO (QE) *ab-initio* package [31]. Geometry optimizations of the atomic positions for the supercells were carried out by using the Broyden-Fletcher-Goldfarb-Shano (BFGS) algorithm [32]. Core-valence electron interactions were described by ultrasoft pseudopotentials. The Kohn-Sham electronic states were expanded in plane-waves up to a kinetic energy cutoff of 30 Ry (1

Ry=13.6 eV) and 240 Ry for the charge density cutoff. The Perdew-Burke-Ernzerhof (PBE) form of the generalized gradient approximation was used to calculate the exchange and correlation contributions. Integrals over the Brillouin-zone were performed by sums of 2 x 2 x 1 Monkhorst-Pack [33] *k*-mesh grid, using the Marzari-Vanderbilt cold-smearing scheme [34] with a broadening of 0.01 Ry. Self-consistency was achieved when the force applied on each atom was less than $1x10^{-3}$ Ry/Bohr and the variation of the total energy between two consecutive iterations was on the order of $1x10^{-4}$ Ry. The electronic density of states (DOS) were calculated within the tetrahedron method using a symmetric 4x4x4 mesh [35]. The lattice parameters obtained after optimization using a 12x12x12 Monkhorst-Pack [33] grid for both bulk carbide and nitride respectively, 4.472 Å and 4.406 Å, are in excellent agreement with experimental data (4.470 Å and 4.390 Å, respectively) [90].

The surfaces used to investigate the thiophene adsorption were modeled employing periodic boundary conditions (PBC). For that, the elementary 2-atomic (*NaCl*-type structure) primitive unit cell vectors were periodically translated twice along the main crystallographic axes (x, y and z), then an adsorbed thiophene molecule was included onto only one side per (2 x 2) surface, corresponding to a coverage of 0.062 ML. The supercell has a dimension of 8.97Å × 8.97 Å × 23.97 Å and the slab was divided into four atomic layers. The supercell height of 23.97 Å yields a vacuum region of ~15 Å along the z-axis, able to avoid spurious interactions between adjacent periodic replicas. In each case, surface relaxation was taken into account and the two topmost layers together with the thiophene molecule were allowed to fully relax on the supercell surface, while the bottom two layers were kept fixed in their bulk positions so that to represent a semi-infinite bulk crystal. As implemented in QE, dipole corrections [38] were applied in order to cancel long-range dipole interactions caused by a charge rearrangement on the surface due to thiophene adsorption and interactions between the two surfaces of the slab. An independent

test of convergence with one additional substrate layer and denser k-point sampling (3 x 3 x 1) was performed, producing only small changes in the adsorption energy and no appreciable changes in the geometric parameters. Consequently, the calculation methods employed here are reasonable and the theoretical results are reliable.

The adsorption (or binding) energies, E_{ads}, were calculated according:

$$E_{ads} = E_{clean+Th} - (E_{clean} + E_{Th})$$

in which the first term in the right-handed side, $E_{clean+T}$, denotes the calculated energy of the slab plus the adsorbed thiophene molecule, whereas E_{clean} and E_{Th} refers to the total energy of the clean NbC and NbN surfaces and the gas-phase thiophene, respectively. Accordingly, an exothermic adsorption is characterized by a negative E_{ads}. A single k point was used in the calculations for the gas phase thiophene, optimized in a large cell (15 x 15 x 15 $Å^3$) which ensures negligible intermolecular interaction and provides good agreement between calculated and experimental data [75]. It is important to point out that the commonly used DFT exchange-correlation functionals (PBE, for example) tend to underestimates adsorption energies because formally they do not take van der Waals (vdW) dispersion forces into consideration. Sony *et.al.,* for example, observed that the inclusion of vdW interactions could significantly influence the adsorption energy of thiophene over Cu(110) [67]. On the other hand, it was also observed that the inclusion of long-range dispersion forces do not improve substantially the resulting orientations and other properties (charge density, electronic states and work function) when results for some aromatics like furan and thiophene, obtained by standard DFT-GGA calculations, to those obtained from experimental data [66-68] are compared. Furthermore, Moses and his collaborators [46] showed that the inclusion of vdW interactions in the adsorption and reaction profile of thiophene on MoS_2 lead to a constant lowering of the energy

differences of the entire reaction path, which in turn was not affected by vdW interactions. Hence, the results reported here suggest that the chosen theoretical method is adequate, since the use of PBE was also to facilitate consistent comparison with similar works. Although systematic calculations using vdW [69-71] and semiempirical (DFT-D) [72,73] density functionals are beyond the scope of the present work mainly due to the highly demanding computational cost, they will be the target of future works.

The climbing-image nudged elastic band (CI-NEB) method [39,41], a robust and efficient approach for the searching of reaction paths, was used as implemented in Quantum-ESPRESSO along with the *quasi*-Newton optimization scheme from Broyden [31] in order to locate energy barriers and transitions states (TS) through the minimum energy path (MEP) by connecting two minima, initial (IS) and final (FS) states. To locate the configurations of maximum energy along the MEP, which climbs uphill to the saddle point and are identified as the TS, we specified several images (typically with six to eight images) of the elementary steps which span the space between the optimized reactant and product configurations. Then, the activation energy (E_A) was estimated to be the energy difference between TS and IS.

Because we are firstly interested in the determination of the energetically most stable adsorbate/surface configuration it is necessary to compare different adsorption orientations and their respective energies. Accordingly, Fig. S.2 (Supporting information – SI) gives an overview of several possible starting adsorption geometries. In the first type, termed “flat” or “η-5”, the thiophene molecular ring is parallel to the surface bonded through its π-system. On the other hand, the terminology “upright” or “η-1” characterizes thiophene in a vertical position relative to the surface and bonded through the sulfur (S) lone pair of electrons. Thus, after testing different adsorption sites and a total of twenty different structures the most stable adsorption complexes were found for the surfaces, NbC(001) and NbN(001), ten

in a η-1 (upright) and ten in a η-5 (flat) configurations. Structures and adsorption energies of the energetically most stable structures are listed in Table 1. As far as we can tell, this is the first theoretical study devoted to the catalytic desulfurization properties of niobium carbides and nitrides.

3. RESULTS AND DISCUSSION

The results reported here are divided into two main parts: in section 3.1, geometries and energies involved in the adsorption process of thiophene on both surfaces, NbC(001) and NbN(001), have been investigated considering only the energetically most stable structures; in section 3.2 we make use of these structure to assess the elementary steps involved in the direct desulfurization process (DDS) of thiophene and in the hydrodessulfurization (HDS) pathways of thiophene H-derivatives, relying principally on the possible structures present at HDS conditions; the reaction steps investigated here were successfully explored in a variety of other computational studies [29,46,74,79,82]. Moreover, a detailed description of the hydrogen dissociation over both surfaces, hydrogenation paths and hydrogenated derivatives can be found in SI. Finally, in section 4 we summarize our conclusions.

3.1. On the structure and energetics of thiophene adsorption - Fig. 1 (left panel) depicts the most stable structure found for the Th/NbC(001) adsorption complex. The energetics of the other evaluated configurations (see Fig. S.2) can be found in Table S.2. As seen, thiophene adsorbs preferentially in a η-1 configuration with the molecular ring tilted up by an angle of ~36° to the surface-parallel plane, with the S atom in the binding position to a surface Nb site. It is interesting to note that before optimization the S atom was directly bonded (η-1) to a surface C atom with initial bond length (BL) of 1.40 Å. However, after successive SCF iterations the molecular ring became tilted and displaced further away from its initial position. Then, in order to test this result we varied the initial thiophene-surface (S-$C_{surface}$) BL to smaller

(0.9 Å, 1.0 Å, 1.3 Å) and to larger (1.7 Å, 1.8 Å and 2.0 Å). The resulting calculations led essentially to the same effect, with only slight differences on the total energy. It can be clearly seen that the molecular ring does not fully interact with the surface, corresponding to a relatively weak adsorption energy of -0.42 eV and producing a S-Nb bond distance of 2.813 Å after optimization.

Figure 1

It was also observed that the adsorption of thiophene on the clean NbC(001) surface causes negligible stretching on the S-C^2, S-C^5 and C^3-C^4 bonds, 1.727 Å, 1.725 Å and 1.428 Å, respectively, after adsorption, whereas C^2-C^3 and C^4-C^5 were slightly shortened decreasing from 1.372 Å in the gas phase to 1.367 Å in the adsorbed phase. Recently, Zhu *et.al.* observed that the adsorption of thiophene on Pt(111) weakens intramolecular bonds and correlated this fact with a loss of aromaticity [74]. Our calculations show no indications of changes in the ring aromaticity after adsorption over NbC(001), but we have found results analogous to those reported for the adsorption of thiophene on both the δ-MoC(001) and TiC(001) surfaces [49,76]. On the other hand, it is known that, contrary to noble metals (Pt, for instance) [78], NbC is highly resistant to poisoning by S [22] probably because it cannot form strong bonds with the surface atoms. Our DFT energy calculations performed and obtained *via* $E_{ads}(S)=[(E_{(S/NbC)}+E_{(H2)})-(E_{(NbC)}+E_{(H2S)})]$ confirm this observation and show that S forms relatively weak covalent bonds with surface Nb and C atoms with adsorption energy [$E_{ads}(S)$] of, -0.34 eV and -072 eV, respectively, which is in qualitative agreement with experiments [22].

Fig. 1 (right panel) indicates the most important properties of the energetically most favorable Th/NbN(001) structure. Contrary to the case of NbC(001), thiophene adsorbs on NbN(001) preferentially in a flat (η-5) orientation with corresponding adsorption energy of -1.10 eV. In this case, the molecular

ring lies roughly centered above a top layer nitrogen atom. Thiophene is slightly distorted out-of-plane after optimization and the S atom is pointed to a surface Nb atom (BL=2.642 Å). Furthermore, S-C^2 and S-C^5 bonds were substantially elongated, from 1.716 Å in the gas phase to 1.852 Å and 1.861 Å, respectively, after adsorption. Moreover, both C^2-C^3 and C^4-C^4 were extended from 1.372 Å to 1.474 Å and 1.479 Å, respectively, whereas C^3-C^4 was shortened from 1.420 Å (gas) to 1.366 Å. Thus, the adsorption has a clear effect on the loss of aromaticity due to a considerable elongation of bonds S-C^2 (Δ=+0.14 Å) and S-C^5 (Δ=+0.15 Å) as well as of C^2-C^3 (Δ=+0.10 Å) and C^4-C^5 (Δ=+0.11 Å). The same effect was also observed by other authors using different surfaces [43,62,74,82].

In the case of monohydrothiophene (MHTh) one hydrogen atom is initially added either on C^2 (2-MHTh) or on C^3 (3-MHTh) of thiophene, allowing the remaining π-bond system to stay unaltered. Our DFT calculations show that the first hydrogenation occurs preferentially on the C^2 atom to form 2-MHTh with an adsorption energy of -1.55 eV. The formation of 2-MHTh/NbC(001) (Fig. S.3-SI) is energetically more stable than that of the 3-MHTh/NbC(001) by 0.51 eV. The formation of 2-MHTh significantly stretches both S-C^2 and S-C^5, from 1.716 Å (gas) to 1.843 Å and to 1.838 Å, respectively. Furthermore, C^2-C^3 and C^4-C^5 were also elongated after the first hydrogenation, while C^3-C^4 was slightly shortened from 1.421 Å (gas) to 1.345 Å. For the second hydrogenation step, and assuming that steric hindrance prevents a second hydrogenation on C^2, one can devise four plausible possibilities at least, namely, on the C^3, C^4 or C^5 carbons of 2-MHTh. Interestingly, we have found the energetically most stable structure when the 2,3-dihidrothiophene (2,3-DHTh) specie is formed. However, it was observed that the rupture of the S-C bonds in this specie has a higher activation barrier (1.53 eV, in this case). This bond rupture proved to be unfavorable when compared to the 2,5-DHTh on the carbide surface. Moreover, we have found that both 2,4-DHTh and 2,5-DHTh (Fig. S.4 - SI), are 0.49 eV and only 0.06 eV, energetically less stable than 2,3-

DHTh, respectively. The adsorption of 2,5-DHTh on the NbC(001) surface accounts for an adsorption energy of -0.70 eV. Our DFT results also indicated that the molecular plane remains tilted on the surface plane, while the S-C^2 and S-C^5 bond distances are equivalently long (1.842 Å).

Turning now to the Th/NbN(001) system, our calculations indicate that the first monohydrogenation of thiophene to form 2-MHTh (E_{ads}=-2.17 eV) is 0.35 eV energetically more stable than of the 3-MHTh. Then, considering the 2-MHTh/NbN(001) adsorption complex (Fig. S.5 – SI), it was observed that the intermolecular bond distances have varied substantially. For both S-C^2 and S-C^5 it was elongated from 1.716 Å (gas) to 1.841 Å and 1.851 Å, respectively and from 1.372 Å (gas) to 1.498 Å for C^2-C^3. On the other hand, it remains practically unchanged for C^4-C^5 (Δ=+0.09 Å) and C^3-C^4 (Δ=-0.07 Å). At the second elementary step of hydrogenation, the positions considered were the same as those for the carbide surface. Furthermore, the energetic of both the 2,3-DHTh and 2,4-DHTh systems have been also tested and compared with 2,5-DHTh. Our calculations revealed that the formation of 2,5-DHTh over NbN(001) (Fig. S.6 - SI) has an adsorption energy of -2.17 eV and it is 0.22 eV and 0.21 eV energetically less stable than 2,3-DHTh and 2,4-DHTh, respectively. Although 2,3-DHTh and 2,4-DHTh are, in principle, energetically more stable than 2,5-DHTh, it was found that the first S-C bond scission of both species has higher activation barriers when compared to 2,5-DHTh, thus the latter system (2,5-DHTh/NbN(001)) was chosen to be used in further studies.

As seen, marked differences between the carbide and the nitride surfaces concerning the adsorption process and the reactions of the thiophene molecule were found. The calculations show that thiophene adsorbs more strongly on the nitride surface and the orientation of the thiophene molecule is also well-defined with respect to the surfaces. Moreover, the changes in the intramolecular bonds in comparison

with the gas phase were substantially more pronounced over NbN(001). In this very instance, it was observed a substantial weakening due to the stretching (but not the rupture) the intramolecular bonds reflecting directly on the loss of aromaticity after adsorption. Thus, the knowledge of the electronic density of states (DOS) appears to be useful for further understanding of the thiophene behavior over such a surface. The DOS spectra of clean NbN(001) and of the same structure after adsorption of thiophene as well as of the thiophene molecule, in both the gas and in the adsorbed phases, are shown in Fig. 2. It suggest that a relatively strong interaction occurs involving the hybridization between the S 2p states related to the pair of lone electrons of S ($9a_1$ orbital) and the surface Nb d-states because of the disappearance of the peak located in ~-2.6 eV (gas phase) after adsorption. As a consequence, the former $9a_1$ orbital (gas phase) gives place to two neighbor peaks mostly attributable to the thiophene C 2p states. Furthermore, the $1b_1$ symmetry orbital relative to the C-C and the S-C π-states shows a lower peak after the adsorption process which, in turn, illustrates that thiophene also interacts with the surface *via* its π-system [37]. We believe that the effective hybridization of the electronic populations of the surface Nb *d*-bands and the $3b_1$ (LUMO) anti-bonding orbital involving charge transfer from the molecular orbitals and back-donation from the *d*-states is responsible for the weakening of the S-C bonds. These results also bring up an interesting question: are the N atoms of the nitride surface participants in the adsorption process? In order to shed some light on that issue the partial DOS (PDOS – Fig. S.7 - SI) projected onto the N 2p states have been computed. The analysis of the PDOS spectra suggests that apparently this is the case. As it may be qualitatively observed, the main features of the PDOS of the selected surface N atoms for both the clean/NbN(001) and Th/NbN(001) systems are quite different, suggesting that these atoms in distinct environments would not act merely like spectators during the adsorption but instead they might be active participants in the process. Accordingly, the PDOS (Fig. S.8 - SI) of the surface Nb atoms projected onto

the d-states show substantial differences between them, meaning that the metallic states are the major factors responsible for the molecule-surface interaction. Obviously, these results are not conclusive and, since the adsorption phenomena depend on the electronic state of the surface, a more detailed analysis is further necessary. Accordingly, additional theoretical studies are now in progress and will be reported in the future.

Figure 2

Contrarily, the η-1 configuration over NbC(001) produces minimal changes on the thiophene intramolecular bond structure and show some similarity with results obtained for a cluster-model of MoS_2 [37]. Our calculations have also indicated that the surface C atoms moved slightly (Δz=+0.033 Å) outwards while the metal atoms moved considerably towards the inside (Δz=-0.114 Å) producing a "zigzag" effect which is in agreement with the experimental STM data and LEED patterns [77]. Therefore, the approximation of the thiophene molecule to the NbC(001) clean surface may be difficult to achieve due to the corrugation of the surface C atoms, causing steric hindrance [49]. This effect might explain why, after being optimized from a surface C site, thiophene prefers to bind *via* its S end at a surface Nb atom in a tilted manner which also represents the configuration that maximizes the interaction of the aromatic system with the surface. The DOS spectra of the NbC(001) systems and of thiophene in both the gas and in the adsorbed phases are depicted in Fig. 3. The clean NbC(001) structure is characterized mainly by low energy C 2s states plus two more important higher energy regions that can be attributed to the hybridization between the Nb d and C p-states, ensuring that chemical bonds occurs principally between Nb and C atoms, in agreement with Maxsimov *et.al.* [81]. The Nb d-states fall just above the Fermi level (E_{fermi}), whereas after thiophene adsorption the DOS around the E_{Fermi} shifts slightly down suggesting a

very modest electron depletion in the Nb d-states and consequently an interaction between the Nb d and the S p-states. As observed in Fig. 3, the adsorption process has also some influence on the electronic structure of thiophene, suggesting that the aromatic character is maintained and that the C atom in the methyne group (CH) is kept in the sp^2-hybridized state because there are no interactions with the surface *via* the π-orbitals [43,53,62,74]. Additionally, a rather subtle change in the DOS near E_{fermi} after the adsorption indicates that the $8a_1$ symmetry orbital, corresponding to the S lone pair of electrons as well as the π-system related to the $1a_1$, $1b_1$ and $2b_1$ (bonding C-C and S-C π-states) orbitals are the responsible for the weak interaction of thiophene with the surface through the overlapping with the Nb d-states, obviously when not taking the vdW forces into consideration. Moreover, a qualitative analysis of the surface Nb atoms PDOS spectra (Fig. S.9 - SI) also present only slight differences before and after thiophene adsorption, corroborating the small transfer of electron density between the surface and the molecule. Interestingly, in this case we notice that the surface C atoms may also play a role in the adsorption process. The analysis of the PDOS (Fig. S.10 - SI) shows qualitative differences of electronic structure for the surface C atoms before and after adsorption takes place, which can be attributed to the transfer of electron density from Nb to C. An analogous behavior was observed by Liu *et.al.* [49] for the adsorption of S-compounds on molybdenum carbides. They pointed out that the metal atoms become more inert due to the effect known as "ligand effect" which is mainly characterized by a downward energy change of the metal *d*-bands [49,87,88] due to transfer of electronic density.

Figure 3

3.2. DDS and HDS processes on *NbC(001)*

3.2.1. DDS of thiophene - We started by testing the DDS pathway, which consist of two subsequent bond scissions (S-C^2 and S-C^5) and no participation of hydrogen species. More informations on the structural parameters can be found in Table S.1 (SI). The relative energies were calculated with respect to the Th/NbC(001) adsorption complex and the zero of energy was set at initial adsorbed state. Fig. 4 depicts the energetic profile of both S-C_2 and S-C_5 bonds scission. Here we assume that the formation of thiolate-like specie stabilizes the system after the first S-C_2 bond scission, as pointed out by experiments [84]. For this process we have found endothermic reaction energy of 0.92 eV with a corresponding activation barrier of 1.74 eV. We also found that the S-C^2 bond was broken at the TS of this step ($TS^1_{DDS\text{-}Carb}$) whereas the S-C^5 bond was slightly elongated from 1.725 Å to 1.734 Å. At the $TS^1_{DDS\text{-}Carb}$ the dissociating S-C^2 bond starts to interact with a surface Nb atom through the thiophene C_2 (BL=2.687 Å). The remaining bond distances, C^2-C^3, C^3-C^4 and C^4-C^5, remain similar to the corresponding initial adsorbed phase. In the second half of the DDS process, the formation of the separated ($S+C_4H_4$) species occurs, and the $TS^2_{DDS\text{-}Carb}$ shows that the S-C^5 bond, with length of 2.491 Å, is already broken. In the final state, the process is endothermic with reaction energy of 0.87 eV along with a corresponding high reaction barrier of 0.90 eV.

Figure 4

3.2.2. HDS of 2-MHTh **-** In a mechanism known as "hydrogenation pathway" (HYD) the scission of the S-C bond is preceded by the hydrogenation of one or more molecular C atoms [4,85]. Thus, after the adsorption of thiophene the first hydrogenation occurs at the ring C^2 atom to form the 2-MHTh/NbC(001) system; the S-C^2 bond is subsequently broken forming an *cis*-butadienethiolate specie. Despite the possibility of the first bond scission occurring at the non-hydrogenated part (S-C^5), Zhu *et.al.* observed that this process is kinetically and thermodynamically less favorable because of the higher activation barrier

and lower reaction energy [74]. Therefore, the first S-C bond scission was investigated only at the hydrogenated (S-C^2) part, as illustrated in Fig. 5. In this case, the relative energies were calculated with respect to the 2-MHTh/NbC(001) system. Accordingly, for the first elementary step we have found activation energy of 1.08 eV and exothermic reaction energy of -0.22 eV. At the transition state ($TS^1_{HYD\text{-}1\text{-}Carb}$) the S-$C^2$ bond is already broken and the molecular ring is rotated from its initial position towards the surface, although it does not became parallel due to steric effects between the thiophene C^2H_2 group and the top Nb atom. The final product is marked by the formation of a thiolate-like system through an intra-rotation of the molecular C^2H_2 group. The equilibrium S-C^2 bond distance was found to be 3.323 Å. The second bond cleavage occurs through the breaking of the S-C^5 bond without prior hydrogenation. It is interesting to note that the $TS^2_{HYD\text{-}1\text{-}Carb}$ is reached along the formation of the C^5-Nb bond and that the molecular hydrocarbon system tends to attain a *trans* configuration in order to reduce the total energy. However, such a process was characterized by a high activation barrier of 2.50 eV and by a strong endothermic reaction energy of 1.14 eV.

Figure 5

3.2.3 HDS of 2,5-DHTh – Here, we considered the 2,5-DHTh/NbC(001) system, from which the relative energy values were calculated. The scission of the S-C^2 bond in 2,5-DHTh is the starting point of the desulfurization process which is followed by the rupture of the S-C^5 bond and then the process leads to the co-adsorbed species, namely, S and C_4H_6 (butadiene). Energies and structures involved, including the transition states for the first and the second bond scission ($TS^1_{HYD\text{-}2\text{-}Carb}$ and $TS^2_{HYD\text{-}2\text{-}Carb}$, respectively), are shown in Fig. 6. Upon the rupture of the S-C^2 bond the $TS^1_{HYD\text{-}2\text{-}Carb}$ shows rotation of the C^2H group and of the molecular ring. In the final state, one can observe the interaction between the C^2 atom and a surface

Nb atom. This process was found to be energetically favorable since calculations indicate exothermic reaction energy of -0.33 eV with corresponding activation energy of 1.27 eV. The second step is the rupture of the S-C^5 bond, and $TS^2_{HYD\text{-}2\text{-}Carb}$ is characterized by an internal rotation of the C^5H_2 group. The final step yields the co-adsorbed S+C_4H_6 species with reaction energy of -0.16 eV and an activation barrier of 1.28 eV.

Figure 6

3.3. DDS and HDS processes on *NbN(001)*

3.3.1. DDS of thiophene – For this study, the relative energies were calculated with respect to the Th/NbN(001) system while the zero of energy was set at initial adsorbed state. As can be seen, in the transition state of the first step ($TS^1_{DDS\text{-}Nitr}$) the S-C_2 bond is broken whereas S-C^5 was slightly shortened from 1.861 Å to 1.783 Å (Table S1). For this step, an activation barrier of 0.90 eV was found along with a slightly exothermic reaction energy (E_R=-0.08 eV). In order to shed light on the formation of the co-adsorbed S and C_4H_4 species we have also evaluated the reaction steps involved in the second S-C bond cleavage (specifically S-C^5), as detailed in Fig. 7. We noticed that the scission of S-C^5 constitutes the rate-determining step of the reaction, $C_4H_4S \rightarrow S+C_4H_4$, with an activation barrier of 0.92 eV and an exothermic energy of -0.22 eV.

Figure 7

3.3.2. HDS of 2-MHTh - In this section, we firstly evaluate the potential energy surface of the S-C^2 bond scission of the 2-MHTh/NbN(001) adsorption complex, from which the relative energy values were obtained, and then the subsequent rupture of the non-hydrogenated S-C^5 bond along with the transition

states ($TS^1_{HYD\text{-}1\text{-}Nitr}$ and $TS^2_{HYD\text{-}1\text{-}Nitr}$). As depicted in Fig. 8, the S-C^2 bond in the $TS^1_{HYD\text{-}1\text{-}Nitr}$ is similar (2.436 Å) when compared with carbide (2.442 Å), whereas the C^2H_2 group is slightly rotated. This elementary step accounts for an activation energy of 1.08 eV and a total exothermic reaction energy of -0.16 eV. If on the one hand our DFT calculations shows that the breaking of the hydrogenated part of 2-MHTh is energetically favorable, on the other hand the scission of the non-hydrogenated bond (S-C^5) is kinetically and thermodynamically less favorable, with an activation barrier and endothermic reaction energy of 1.43 eV and 0.95 eV, respectively.

Figure 8

3.3.3. HDS of 2,5-DHTh - The HYD pathway for the 2,5DHTh/NbN(001) adsorption complex is shown in Fig. 9. This process initiates by the breaking of the S-C^2 bond leading to formation of *cis*-2-butenethiolate *via* transition state ($TS^1_{HYD\text{-}2\text{-}Nitr}$), accounting for an activation energy of 1.07 eV and an exothermic reaction energy of -0.51 eV. During this step the molecular ring tilts slightly down towards the surface-parallel plane. At $TS^1_{HYD\text{-}2\text{-}Nitr}$ the S-C^2 bond was partially broken (BL=2.582 Å), but it is still distant from the surface Nb atom (BL=3.307 Å). At the end of this step, the C^2H_2 group is covalently linked to Nb_s with a bond distance of 2.313 Å and the length of the S-Nb bond is shortened from 2.786 Å to 2.480 Å. Subsequently, to the formation of the co-adsorbed S and butadiene (S+C_4H_6) species the system has to overcome an energy barrier of 1.53 eV at the $TS^2_{HYD\text{-}2\text{-}Nitr}$ with exothermic reaction energy of -0.30 eV. At the $TS^2_{HYD\text{-}2\text{-}Nitr}$ the breaking initiates at the S-C^5 bond along with the forming of C^5-Nb, with distances of 2.616 Å and 3.279 Å, respectively. At the final state the C^2-Nb and the C^5-Nb bond distances are 2.320 Å and 2.330 Å, respectively, while the S-Nb length is found to be 2.191 Å.

Figure 9

3.3. Reaction energies, barriers and mechanisms – Figs. 4-9 gives an schematic overview on the reactions involved in the desulfurization pathways of thiophene and its H-derivatives on NbN(001) and NbC(001). The approximations used in this study are justified since, as suggested by experiments, the S-C bond cleavage may be observed prior to the hydrogenation of thiophene by including the surface transition metal *via* covalent bond to stabilize the resulting fragments [36,84]. Accordingly, the double step mechanism of the S-C bond scission, belonging to the DDS pathway, includes the formation of a thiolate-like specie (1^{st} step), and then yields separate species, $C_4H_4S \rightarrow S+C_4H_4$, species ($2^{nd}$ step). It was proposed in the literature that highly reactive species such as thiolates behave as key intermediates in a variety of possible mechanisms regarding desulfurization processes [4,83,84]. Considering in the first place the NbC(001) surface, the scission of S-C[2] (1^{st} step) was found to be endothermic (E_{R1}=0.92 eV) and in some extent kinetically unfavorable (E_A^1=1.74 eV). The 2^{nd} step was found to be less difficult, accounting for an activation barrier (E_A^2) of 0.90 eV but being slightly less endothermic (E_{R2}=0.87 eV) than the 1^{st} step. On the other hand, by considering the behavior of the NbN(001) surface we notice that its desulfurization properties *via* DDS mechanism are in ideal conditions bettered when compared to those from NbC(001). Accordingly, the formation of an energetically stable (η-5) Th/NbN(001) adsorption complex (E_{ads}=1.10 eV) was more efficient in activating thiophene by allowing it to start the dissociation process at a point closer to the surface, so facilitating the S-C bond breaking process and consequently the formation of the stable thiolate specie. This is corroborated by our DFT calculations which showed slightly exothermic reaction energies (1^{st}: E_{R1}=-0.08 eV; 2^{nd}: E_{R2}=-0.22 eV) and activation barriers of (1^{st}) 0.90 eV and (2^{nd}) 0.92 eV for both steps of the DDS pathway.

We assumed that in all systems used to study the dissociation of the S-C bond under hydrogenating conditions (HYD mechanism) an equilibrium between hydrogen molecules (H_2) and adsorbed hydrogen

atoms exists because, as reported in the literature, the dissociation of H_2 is not believed to be the rate determining step in desulfurization reactions [29,36]. Then, in order to assess the catalytic behavior of the surfaces (carbide and nitride), the potential energy diagrams were evaluated separately for each adsorption complex. Accordingly, the analysis of the S-C bond breaking by the HYD mechanism permits to conclude that the niobium nitride surface has, again, a better performance when compared to niobium carbide. Firstly, the breaking of the S-C bond of the monohydrogenated systems (2-MHTh) on NbN(001) imposes for the 1st and 2nd steps of this reaction an energy barrier of 1.08 eV and 1.43 eV, respectively, with the computed reaction energies of -0.16 eV (E_{R1}) and 0.95 eV (E_{R2}), respectively. On the other hand, while the 1st step has an essentially similar energy barrier of 1.08 eV (and E_{R1}=-0.22 eV), in the 2st step the NbC(001) surface imposes a considerably larger activation barrier (E_A=2.50 eV) and yields an energetically unstable system in which the formation energy was computed to be endothermic by 1.14 eV.

The analysis of the complete HYD mechanism (2,5-DHTh/surface) showed a slightly better performance for the nitride surface. The investigation of the S-C bond breaking mechanism of 2,5-DHTh over NbN(001) reveals that the 1st step, which leads to the formation of the *cis*-butadienethiolate species, is favorable when compared with the carbide surface because of the lower activation and reaction energies: E_A^1=1.07 eV (NbN) *vs.* 1.27 eV (NbC); E_{R1}=-0.51 eV (NbN) *vs.* -0.33 eV (NbC). The 2st step is marked by the formation of the co-adsorbed S and butadiene and reveals a favorable pathway to desulfurization over NbN(001). For this step, we found an activation energy of 1.53 eV (E_A^2) along with reaction energy of -0.30 eV (E_{R2}), whereas on the carbide surface this step has an energy barrier of 1.28 eV (E_A^2) along with reaction energy of -0.16 eV (E_{R2}). Although in real conditions both surfaces present lower activities when compared with the catalysts commonly used in desulfurization processes, the results reported here are in qualitative agreement with the experimental data available for similar systems [20,22-24]. It is known that

butadiene is formed from the S-C bond breaking of 2,5-DHTh in a great variety of HDS reactions and catalysts [29,42,45,65]. Notably, Nagai *et.al.* have synthesized niobium nitride supported on γ-Al_2O_3 using the CVD technique for HDS of thiophene, observing activity at ~400°C and atmospheric pressure [20]. On the one hand, they observed that the activity of the catalyst decreases due to the accumulation of S atoms on the Nb sites [20]; this result are in line with our DFT calculations, which indicate the formation of covalent bonds of S with surface Nb atoms with E_{ads}(S)=-1.25 eV. On the other hand, they also correlated the decrease of the catalytic activity with the loss of nitrogen from the nitride surface. This effect was not evaluated in the present study, but studies are now in progress and will be published elsewhere. In spite of the fact that Nagai *et.al.* did not find butadiene as the main product of the reaction, it is known that this specie, in general, undergoes fast hydrogenation and subsequent isomerization to yield principally butenes and butane [20,45]. On the other hand, Ramanathan and Oyama [22] observed better HDS activity of NbC when compared to TiN, VC and VN, but lower activity compared to other TMCNs (Mo_2C, WC and Mo_2N) and commercial catalysts. Thus, the present results provide important clues on why experimentally NbC has not been observed as an effective catalyst for the activation of sulfur compounds for further reactions like those related to desulfurization processes. Unfortunately, to the best of our knowledge further experimental data on the reaction mechanisms on niobium carbides and nitrides are scarce, precluding direct quantitative correlations with the theoretical data. Despite this, we have found some similarities with the desulfurization ability of noble metal platinum surfaces [74,82]. In these noble surfaces it was found, theoretically and experimentally, that the DDS pathway was preferred over HYD in the case of the thiophene desulfurization. Apparently, the same is true to both surfaces studied in the present paper. In the case of the NbN(001), the ring hydrogenations slightly increase the activation barrier of the cleavage of the S-C bond making the dessulfurization through the HYD mechanism more difficult and giving preference to

the DDS mechanism. This result could explain why the NbN(001) surface is more active than NbC(001), since the DDS pathway comprises only two steps, namely, the cleavage of the S-C bonds, to complete the desulfurization process. On the other hand, although the hydrogenation through the HYD pathway was found to lower the activation energy on the NbC(001) surface, which possibly represents an important step to desulfurization, the barrier to this reaction is by itself a difficult step [29,40,62,74,82]. Thus, under the drastic conditions of temperature and pressure that the catalysts are subject in HDS processes, it is acceptable that the C_4H_4 species be formed *via* DDS and readily hydrogenated to form the hydrocarbons commonly identified in these processes [62,74].

4. CONCLUDING REMARKS

In the present periodic DFT study we have studied the adsorption of thiophene and some of its hydrogenated derivatives on the niobium carbide and nitride slabs, which represent the common cubic face-centered (001) surface, as well as investigated the catalytic properties of these surfaces towards desulfurization reactions with different models of adsorbed molecules. Our theoretical calculations suggest the following conclusions.

On the niobium nitride surface thiophene adsorbs preferentially in a η-5 configuration through its π-structure with substantial changes of the intramolecular structure including loss of aromaticity, mostly attributable to the hybridization between the electronic states of thiophene and surface Nb atoms. On the other hand, on the niobium carbide surface the thiophene molecular ring was found to prefer a tilted η-1 configuration, but leading to less pronounced changes of the intramolecular structure, correlated to a modest interaction between the Nb d and thiophene p-states. For the hydrogenated derivatives, the calculated adsorption energies were also exothermic and we observed a ring lifting from the surface as the

number of added hydrogen increase. Based on NEB calculations our results also provide some kinetic and thermodynamic information on catalysts activity for thiophene desulfurization. In NbC(001) a possible low activity might be related to surface effects, namely, the undulation of the surface C atoms which in turn causes steric hindrance, whereas the NbN(001) surface presents deactivation due to the surface S deposition caused by the formation of strong covalent S-Nb bonds. Moreover, the analysis of the electronic effects due to the adsorption has identified the participation in some extent of the non-metal surface atoms in the process. Additionally, the cleavage of the S-C bond of thiophene and its hydrogenated counterparts were analyzed. All cases suggest that the desulfurization starts by the $S\text{-}C^2$ bond breaking, which is then followed by the $S\text{-}C^5$ bond breaking. Based on these studies our theoretical results suggest that for both surfaces the slight reduction of energy barriers caused by ring hydrogenation does not necessarily lead to a preference for the HYD pathway of thiophene desulfurization. As observed, the direct desulfurization (DDS) pathway was found to be preferred. We have also found that in ideal conditions the niobium nitride surface presents a better performance for the desulfurization of thiophene than its "sister" the carbide surface.

5. AKNOWLEDGEMENTS

The work was supported by Conselho Nacional de Desenvolvimento Científico e Tecnológico (CNPq), Coordenação de Aperfeiçoamento de Pessoal de Nível Superior (CAPES) and Fundação de Amparo à Pesquisa do Estado do Rio de Janeiro (FAPERJ).

6. REFERENCES

[1] Stanislaus, A.; Marafi, A; Rana, M.S.; Recent advances in the science and technology of ultra low sulfur diesel (ULSD) production. *Catal. Today* **153** (2010) 1–68.

[2] Song, C.; Hsu, S.; Mochida, I. (Eds.), Chemistry of Diesel Fuels, Taylor & Francis, New York, 2000.

[3] Felipe Sanchez-Minero, F.; Ramırez, J.; Gutierrez-Alejandre, A.; Fernandez-Vargas, C.; Torres-Mancera, P.; Cuevas-Garcia, R. *Catal. Today* **133** (2008) 267–276.

[4] Topsøe, H.; Clausen, B.S.; Massoth, F.E. Hydrotreating Catalysis, Science and Technology, Springer, New York, 1991.

[5] Grange, P.; Vanhaeren, X. *Catal. Today* **36** (1997) 375-391.

[6] Ramos, R.R.; Bolıvar, C.; Castillo, J.; Hung, J.; Scott, C.E. *Catal. Today* **133** (2008) 277–281.

[7] Song, C. in: Proceedings of Fifth International Conference on Refinery Processing, Held in Conjunction with AIChE Spring National Meeting (2000), New Orleans, 11–14 March 2002, pp. 3–12;

[8] Rodriguez, J.A.; Dvorak, J.; Jirsak, T. *Surf. Sci.* **457** (2000) L413-L420.

[9] Levy, R. B., Boudart, M., *Science*, **181** (1973) 547-549.

[10] Berendes, A., Galesic, I., Martens, R., *Z. Anorg. Allg. Chem.* **629** (2003). 1769-1777.

[11] Ranhotra, G. S.; Bell, A. T.; Reimer, J. A. *J. Catal.* **108** (1987) 40-49.

[12] Park, K. Y.; Seo, W. K.; Lee, J. S. *Catal. Lett.* **11** (1991) 349-356.

[13] Rocha, A.S.; Rocha, A.B.; da Silva, V.T. *Appl. Cat. A: Gen* **379** (2010) 54-60.

[14] Lee, J. S.; Yeom, M. H.; Park, K. Y.; Nam, I. S.; Chung, J. S.; Kim, Y. G.; Moon, S. H. *J. Catal.* **128** (1991) 126-136.

[15] Neylon, M.K.; Choi, S.; Kwon, H.; Curry, K.E.;Thompson, L.T. *Appl. Cat. A: Gen.* **183** (1999) 253-263.

[16] Patt, J.; Moon, D. J.; Phillips, C.; Thompson, L. *Catal. Lett.* **65** (2000) 193-195.

[17] Kojima, R.; Aika, K. *Appl. Catal. A: Gen.* **219** (2001) 141-147.

[18] Ledoux, M. J.; Cuong, P. H.; Guille, J.; Dunlop, H. *J. Catal.* **134** (1992) 383-398.

[19] Schwartz, V.; da Silva, V. T.; Oyama, S. T. *J. Mol. Catal. A-Chem.* **163** (2000) 251-268.

[20] Nagai, M.; Nakauchi, R.; Ono, Y.; Omi, S. *Catal. Tod.* **57** (2000) 297-304.

[21] Melo-Bandaa, J.A.; Dominguez, J.M.; Sandoval-Robles, G. *Stud. in Surf. Sci. Catal.* **130** (2000) 2843-2848.

[22] Ramanathan, S; Oyama, S.T. *J. Phys. Chem*. **99** (1995) 16365-16372.

[23] Schwartz, V.; Oyama, S. T.; Chen, J.C. *J. Phys. Chem. B* **104** (2000) 8800-8806.

[24] Chagas, C.A.; Pfeifer, R.; Rocha, A.B.; da Silva, V.T. *Top Catal.* **55** (2012) 910-932.

[25] Kojima, I.; Orita, M.; Miyazaki, E.; Otanis, S. . *Surf. Sci.* **160** (1985) 153-163.

[26] Zhang, Y.F.; Li, J.Q; Zhou, L.X. *Surf. Sci.* **488** (2001) 256-268.

[27] Vojvodic, A.; Ruberto, C.; Lundqvist, B.I. *J. Phys.: Cond. Mat*. **22** (2010) 375504.

[28] Nakane, T.; Noda, T.; Ozawa, K.; Edamoto, K. *Surf. Sci*. **433** (1999) 180-183.

[29] Moses, P.G.; Hinnemann, B.; Topsøe, H.; Nørskov, J.K. *J. Cat.* **248** (2007) 188–203.

[30] Smelyansky, V.; Hafner, J.; Kresse, G. *Phys. Rev. B* **58** (1998) R1782-R1785.

[31] Giannozzi, P. et.al. *J. Phys.: Cond. Mat*. **21** (2003) 395502.

[32] Billeter, S.; Turner, A.; Thiel, W. *Phys. Chem. Chem. Phys.* **2** (2000) 2177.

[33] Monkhorst, H.J., Pack, J.D., *Phys. Rev. B,* **13** (1976) 5188-5192.

[34] Marzari, N., Vanderbilt, D., De Vita, A., Pyne, D., *Phys. Rev. Lett.*, **82** (1999) 3296-3299.

[35] P.E. Blöchl, O. Jepsen, O.K. Andersen, *Phys. Rev. B* **49** (1994) 16223-16234.

[36] Vrinat, M.L. *App. Cat.*, **6** (1983) 137-158.

[37] Rodriguez, J.A. *J. Phys. Chem. B* **101** (1997) 7524-7534.

[38] Bengsston, L. *Phys. Rev. B* **59** (1999) 12301-12304.

[39] G. Mills, H. Jónsson, G.K. Schenter, *Surf. Sci.* **324** (1995) 305-337;

[40] Henkelman, J.; Jónsson, H.; *J. Chem. Phys.* **113** (2000) 9978-9985.

[41] Henkelman, J.; Uberuaga, B.P.; Jónsson, H.; *J. Chem. Phys.* **113** (2000) 9901-9904.

[42] Markel, E. J., Schrader, G. L., Sauer, N. N., and Angelici, R. J., *J. Catal.* **116** (1989) 11-22.

[43] Mittendorfer, F.; Hafner, J. *Surf. Sci.* **492** (2001) 27-33.

[44] Martin Callsen, M.; Atodiresei, N.; Caciuc, V.; Blugel, S. *Phys. Rev. B* **86** (2012) 085439.

[45] Sullivan, D.L. and Ekerdt, J.G. *J. Catal.* **178** (1998) 226–233.

[46]Moses, P.G.; Hinnemann, B.; Topsøe, H.; Nørskov, J.K. *J. Cat.* **268** (2009) 201–208.

[47] Wu, Z.; Li, C.; Wei, Z.; Ying, P.; Xin, Q. J *J. Phys. Chem. B* **106** (2002) 979-987.

[48] Hada, K.; Tanabe J.; Omi, S.; Nagai, M. *J. Cat.* **207** (2002) 10-22.

[49] Liu, P.; Rodriguez, J.A.; Muckerman, J.T. *J. Phys. Chem. B* **108** (2004) 15662-15670.

[50] St. Clair, T. P.; Oyama, S. T.; Cox, D. F. *Surf. Sci.* **511** (2002) 294-302.

[51] Rodriguez, A.; Dvorak, J.; Jirsak, T. *Surf. Sci* **457** (2000) L413-L420.

[52] Zonnevylle, M. C.; Hoffmann, R.; Harris, S. *Surf. Sci.* **199** (1988) 320-360.

[53] Orita, H.; Uchida, K.; Itoh, N. *J. Mol. Cat. A: Chem*. **193** (2003) 197-205.

[54] Liu, G.; Rodriguez, J. A.; Dvorak, J.; Hrbek, J.; Jirsak, T. *Surf. Sci.* **505** (2002) 295-307.

[55] Rousseau, G. B. D.; Bovet, N.; Johnston, S. M.; Lennon, D.; Dhanak. V.; Kadodwala, M. *Surf. Sci.* **511** (2002) 190-202.

[56] Khan, N. A.; Hwu, H. H.; Chen, J. G. *J. Cat.* **205** (2002) 259-265.

[57] Venezia, A. M.; La Parola, V.; Deganello, G.; Cauzzi, D.; Leonardi, G.; Predieri, G. *Appl. Catal. A: Gen.* **229** (2002) 261.-271

[58] Venezia, A.M.; La Parola, V.; Nicoli, V.; Deganello, G. *J. Catal.* **212** (2002) 56-62.

[59] Damyanova, S.; Petrov, L.; Grange, P. *Appl. Catal. A:Gen.* **239** (2003) 241-252.

[60] Jirsak, T.; Dvorak, J.; Rodriguez, J. A. *J. Phys. Chem. B* **103** (1999) 5550-5559.

[61] Liu, G.; Rodriguez, J. A.; Hrbek, J.; Long, B. T.; Chen, D. A. *J. Mol. Catal. A: Chem.* **202** (2003) 215-227.

[62] Mittendorfer, F.,Hafner, J., J. Cat. **214** (2003) 234-241.

[63] Tominaga, H., Nagai, M., *Appl. Cat. A: Gen.* **343** (2008) 95-103.

[64] de Souza,E.F.; Chagas, C.A.; Ramalho, T.C.; da Silva, V.T.; Aguiar, D.L.M.,San Gil, de Alencastro, R.B. *J. Phys. Chem. C* **117** (2013) 25659−25668.

[65] Sauer, N. N., and Angelici, *Inorg. Chem.* **26** (1987) 2160-2164.

[66] Bradley, M.K.; Robinson, J.; Woodruff, D.P. *Surf. Sci.* **604** (2010) 920-925.

[67] Sony, P.; Puschnig, P.; Nabok, D.; Ambrosch-Draxl, C. *Phys. Rev. Let.* **99** (2007) 176401.

[68] Atodiresei, N.; Caciuc, V.; Lazic, P.; Blugel, S. *Phys. Rev. Let.* **102** (2009) 136809.

[69] Dion, M.; Rydberg, H; Schroder, E.; Langreth, D. C.; Lundqvist, B. I. *Phys. Rev. Let.* **92** (2004) 246401.

[70] Thonhauser, T.; Cooper, V. R.; Li, S.; Puzder, A.; Hyldgaard, P.; Langreth, D. C. *Phys. Rev. B* **76** (2007) 125112.

[71] Roman-Perez, G.; Soler, J. M. *Phys. Rev. Let.* **103** (2009) 096102.

[72] F. Ortmann, F. Bechstedt, and W. G. Schmidt, *Phys. Rev. B* **73** (2006) 205101.

[73] S. Grimme, *J. Comp. Chem.* **27** (2006) 1787-1799.

[74] Zhu, H.; Guo, W.; Li, M.; Zhao, L.; Li, S.; Li, Y.; Lu, X.; Shan, H.; *ACS Cat.* **1** (2011) 1498-1510.

[75] a)Harshbarger, W. R.; Bauer, S. H. *Acta Cryst. B* **26** (1970) 1010-1020; b) Bak, B.; Christensen, D.; Hansen-Nygaard, L.; Rastrup-Andersen, J. *J. Mol. Spectr.* **7** (1961) 58-63.

[76] Liu, P; Rodriguez, J.A.; Muckerman and, J.T., *J. Chem.Phys.* **118** (2003) 7737-7740.

[77] Tsong, R.M.; Schmid, M.S.; Nagl, C., Varga, P.; Davi, R.F.; Tsong, I.S.T. *Surf. Sci.* **366** (1996) 85-92.

[78] Yoshimura, Y.; Toba, M.; Matsui, T.; Harada, M.; Ichihashi, Y.; Bando, K. K. *Appl. Catal. A:Gen* **322** *(*2007) 152-171.

[79] Logadottir, A.; Moses, P.G.; Hinnemann, B.; Topsøe, N.; Knudsen, K.G.; Topsøe, H.; Nørskov, J.K. *Cat. Today* **111** (2006) 44–51.

[80] Mittendorfer, F and Hafner, J. *J. Phys. Chem. B* 2002, **106**, 13299-13305.

[81] E. G. Maksimov, S.V. Ebert, M. V. Magneistkay and A.E. Karakozov, *J. Exp and Theo. Phys*., **105** (2007) 642.

[82] Zhu, H.; Lu, X.; Guo, W.; Li, L.; Zhao, L.; Shan, H. *J. Mol. Cat. A: Chem*. **363** (2012) 18–25.

[83] H. Schulz, M. Schon, H.M. Rahman, in: L. Cerveny (Ed.), Studies in Surface Science and Catalysis, Elsevier, Amsterdam, 2000, p. 204.

[84] Chen, J.; Daniels, L.M.; Angelici, R.J. *J. Am. Chem. Soc.* ***113*** (1991) 2544-2552.

[85] E.J.M. Hensen, M.J. Vissenberg, V.H.J. de Beer, J.A.R. van Veen, R.A. Van Santen, *J. Catal.* **163** (1996) 429-435.

[86] Vorotnikov, V.; Mpourmpakis, G.; Vlachos, D.G. *ACS Cat.* **2** (2012) 2496−2504.

[87] Liu, P.; Rodriguez, J. A. *J. Chem. Phys.* **120** (2004) 5414-5423.

[88] Liu, P.; Rodriguez, J. A. *Catal. Lett.* **91** (2003) 247-252.

[89] de Souza,E.F.; Chagas, C.A.;Ramalho, T.C.; de Alencastro,R.B. *Dalt. Trans.* **41** (2012) 14381−14390.

[90] Toth, L.E. Transition Metal Carbides and Nitrides Academic Press, New York (EE.UU.) (1971).

FIGURE CATPTIONS

Figure 1 - Optimized configurations of the most stable structures for the thiophene(Th)/NbC(001) (right panel) and the Th/NbN(001) (left panel) adsorption systems. The optimized configurations are referred to the initial positions 1 (η-1) and 5 (η-5) over carbide and nitride, respectively (see Fig. S.1).

Figure 2 – Total electronic density of states (DOS) for the niobium nitride surfaces and thiophene before (NbN_{clean} and Th_{gas}) and after the adsorption process takes place and considering the energetically most stable structure.

Figure 3 – Total DOS for the niobium carbide surfaces and thiophene before (NbN_{clean} and Th_{gas}) and after the adsorption process takes place and considering the energetically most stable structure.

Figure 4 – Reaction pathway and relative energy profile for the direct desulfurization of the thiophene molecule on the carbide surface. The reference energy is thiophene on the NbC(001) and thiophene in the gas phase. The inset shows the possible structures of the calculated transition states ($TS^{1,2}_{DDS\text{-}Carb}$), intermediate and final product.

Figure 5 - Relative energy diagram for the hydrodesulfurization of the 2-monohydrothiophene on the carbide surface. The reference energy is 2-monothiophene (2-MHTh) on the NbC(001) surface and the same molecule in the gas phase. The inset shows the possible structures of the calculated transition states ($TS^{1,2}_{HDS\text{-}Carb}$), intermediate and final product.

Figure 6 - Relative energy diagram for the hydrodesulfurization of the 2,5-dihydrothiophene on the carbide surface. The reference energy is 2,5-dihydrothiophene (2,5-DHTh) on the NbC(001) surface and the same molecule in the gas phase. The inset shows the possible structures of the calculated transition states ($TS^{1,2}_{HDS\text{-}Carb}$), intermediate and final product.

Figure 7 - Reaction pathway and relative energy profile for the direct desulfurization of the thiophene

molecule on the nitride surface. The reference energy is thiophene on the NbN(001) and thiophene in the gas phase. The inset shows the possible structures of the calculated transition states ($TS^{1,2}_{DDS\text{-}Nitr}$), intermediate and final product.

Figure 8 - Relative energy diagram for the hydrodesulfurization of the 2-monohydrothiophene on the nitride surface. The reference energy is 2-monothiophene on the NbN(001) surface and the same molecule in the gas phase. The inset shows the possible structures of the calculated transition states ($TS^{1,2}_{HDS\text{-}Nitr}$), intermediate and final product.

Figure 9 – Reaction pathway for the hydrodesulfurization of the 2,5-dihydrothiophene on the nitride surface. The reference energy is 2,5-dihydrothiophene on the NbN(001) surface and the same molecule in the gas phase. The inset shows the possible structures of the calculated transition states ($TS^{1,2}_{HDS\text{-}Nitr}$), intermediate and final product.

FIGURES

Figure 1

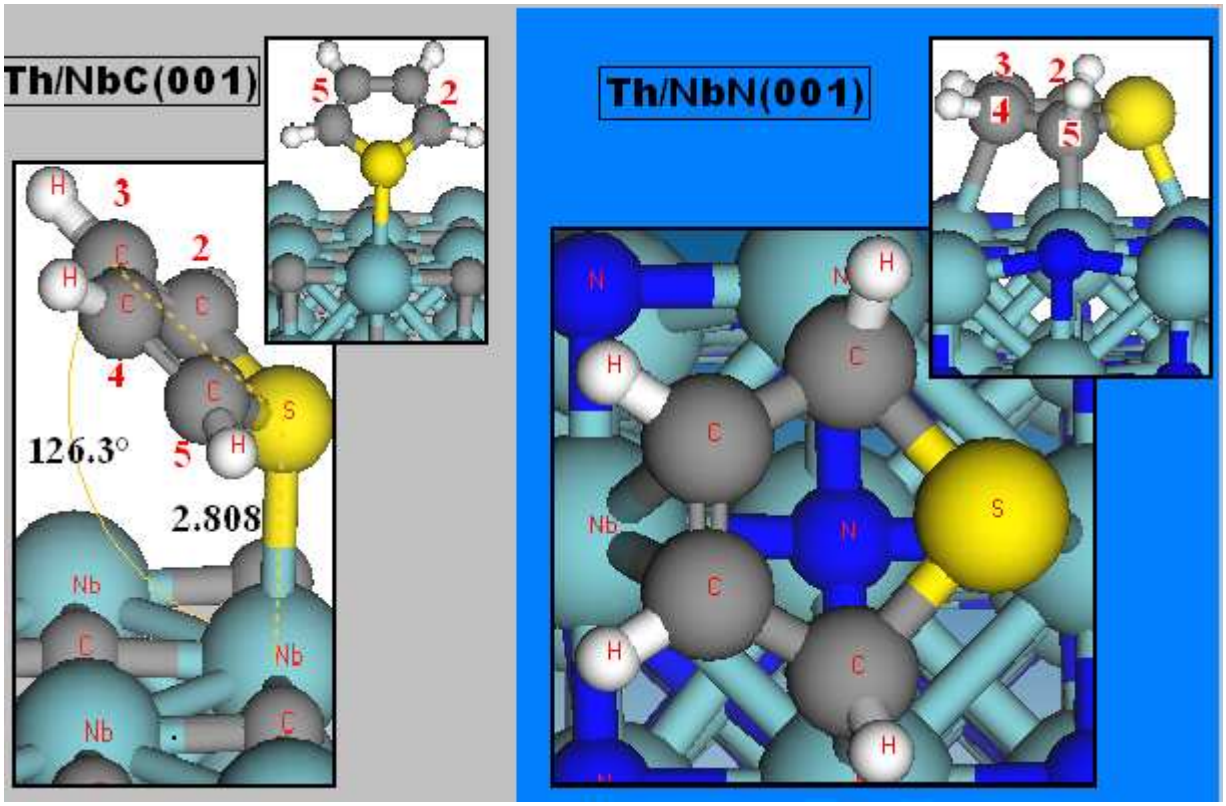

Figure 2

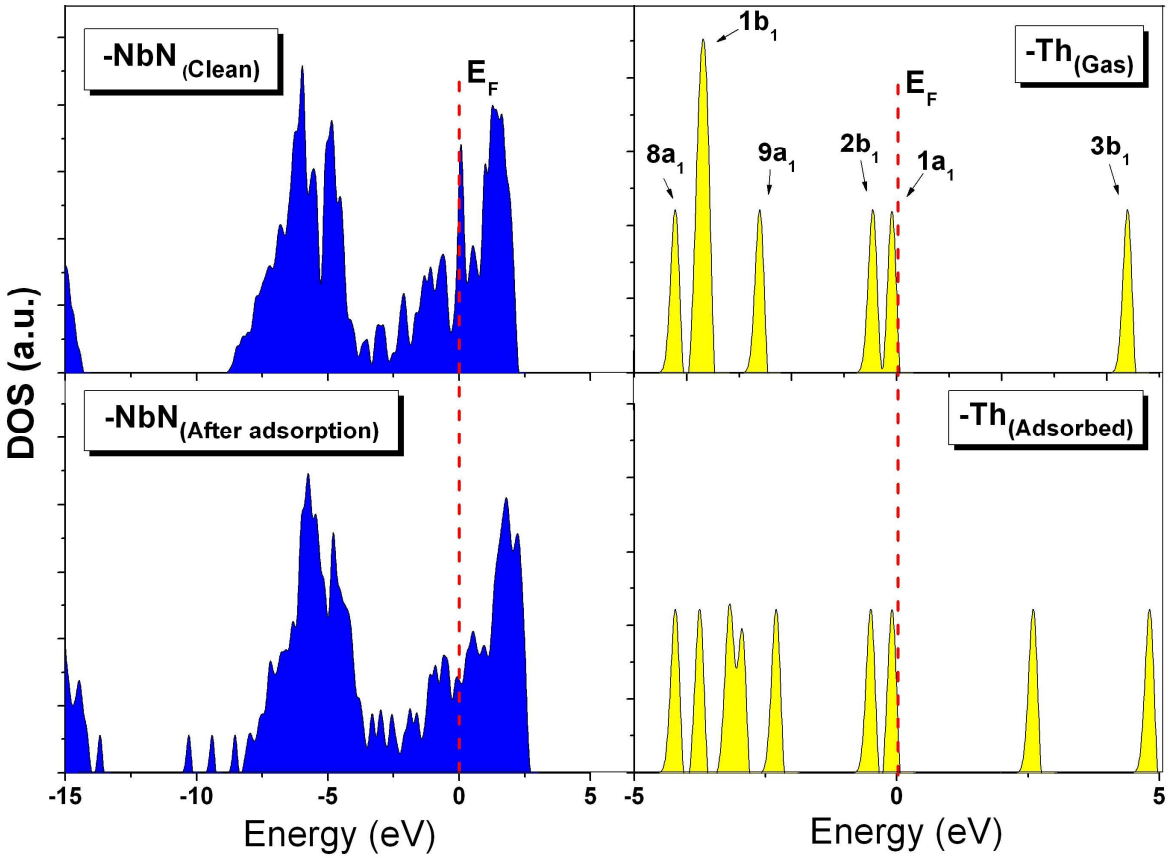

Figure 3

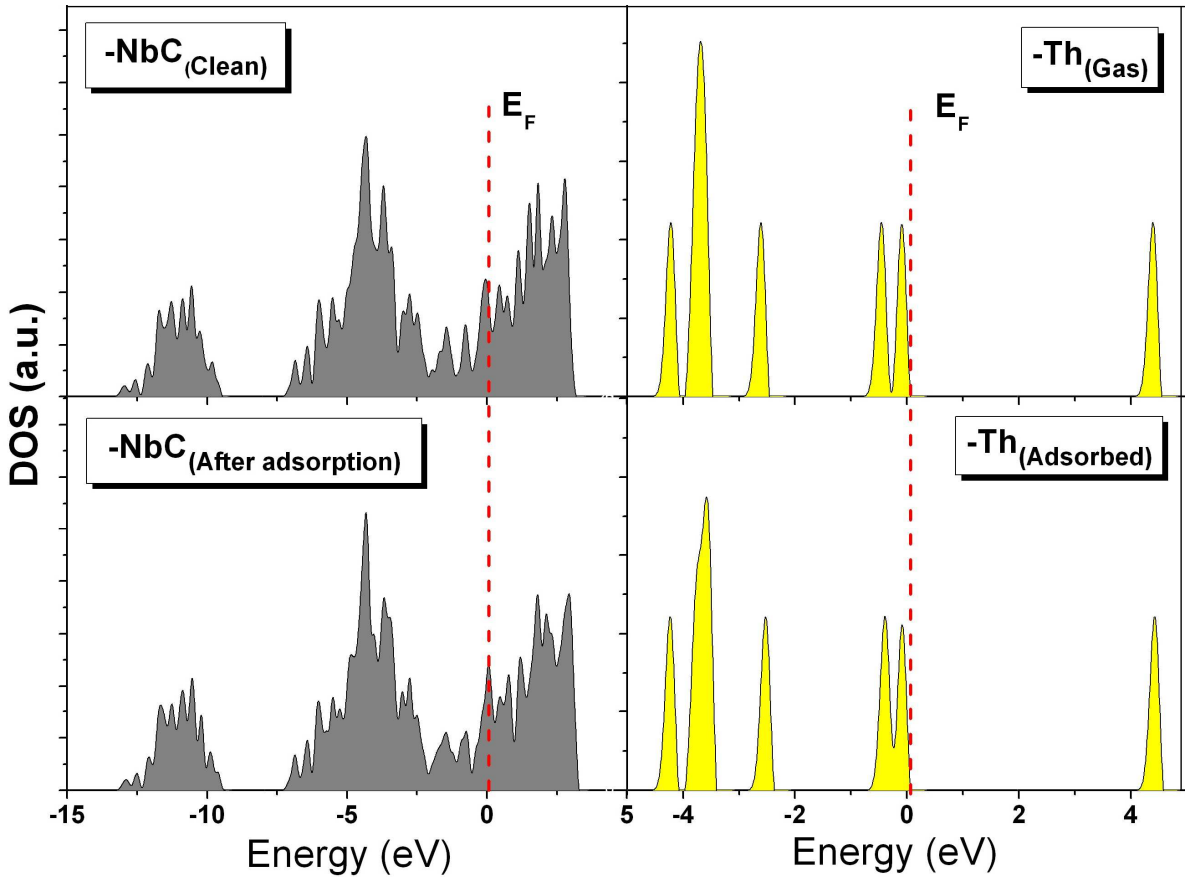

Figure 4

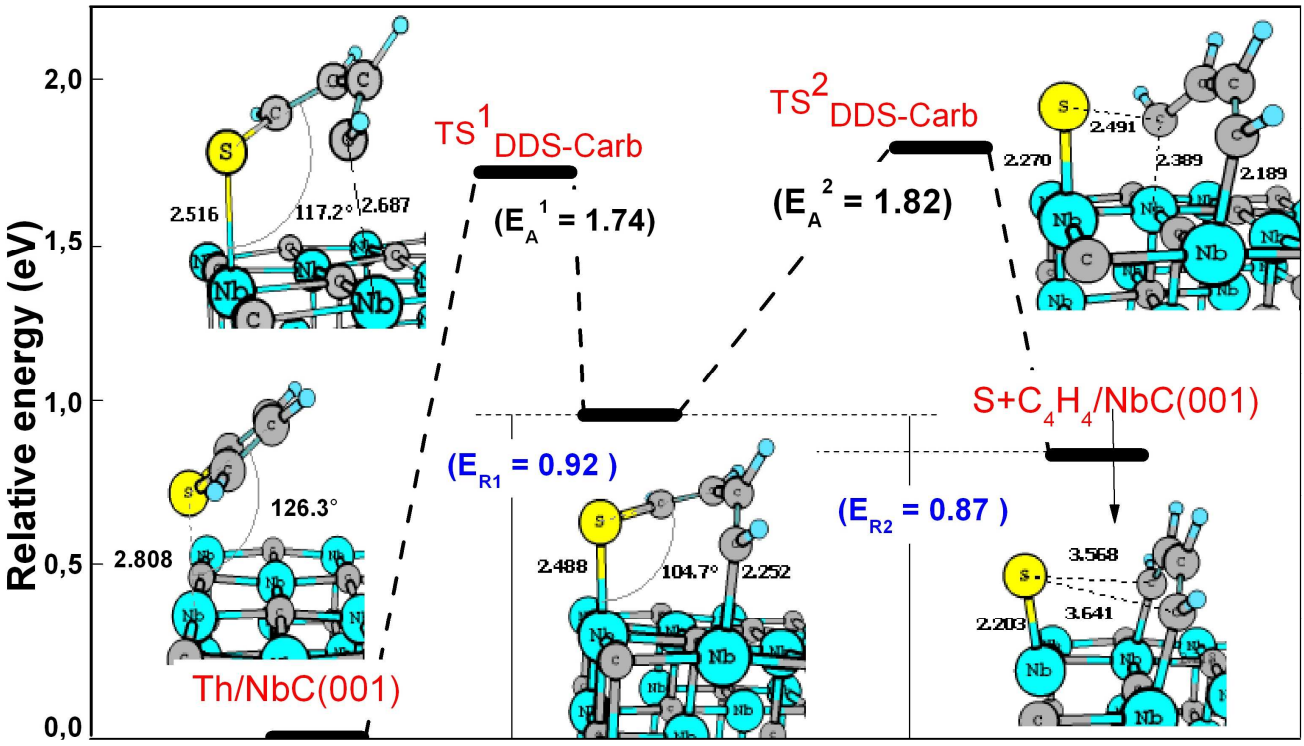

Figure 5

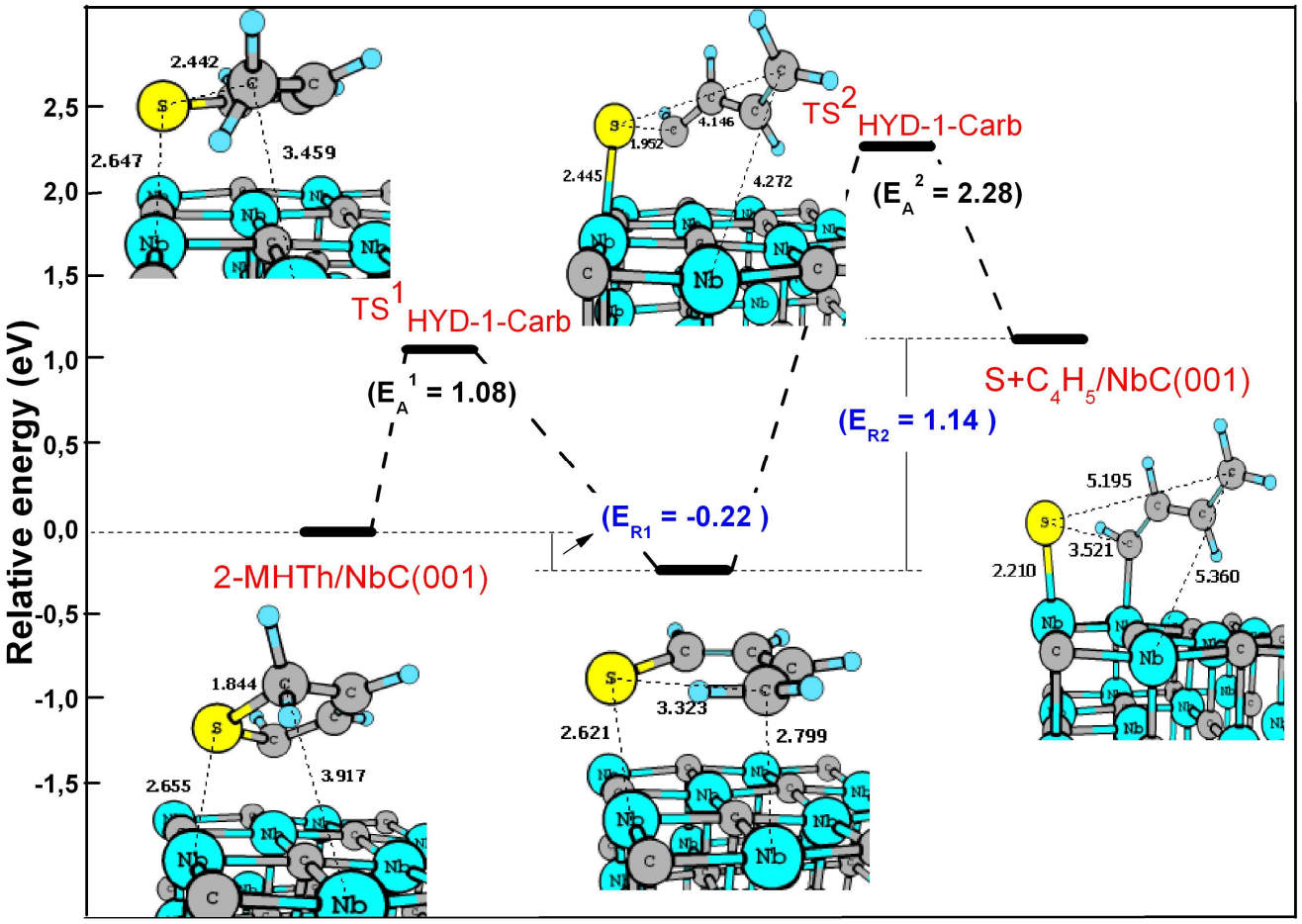

Figure 6

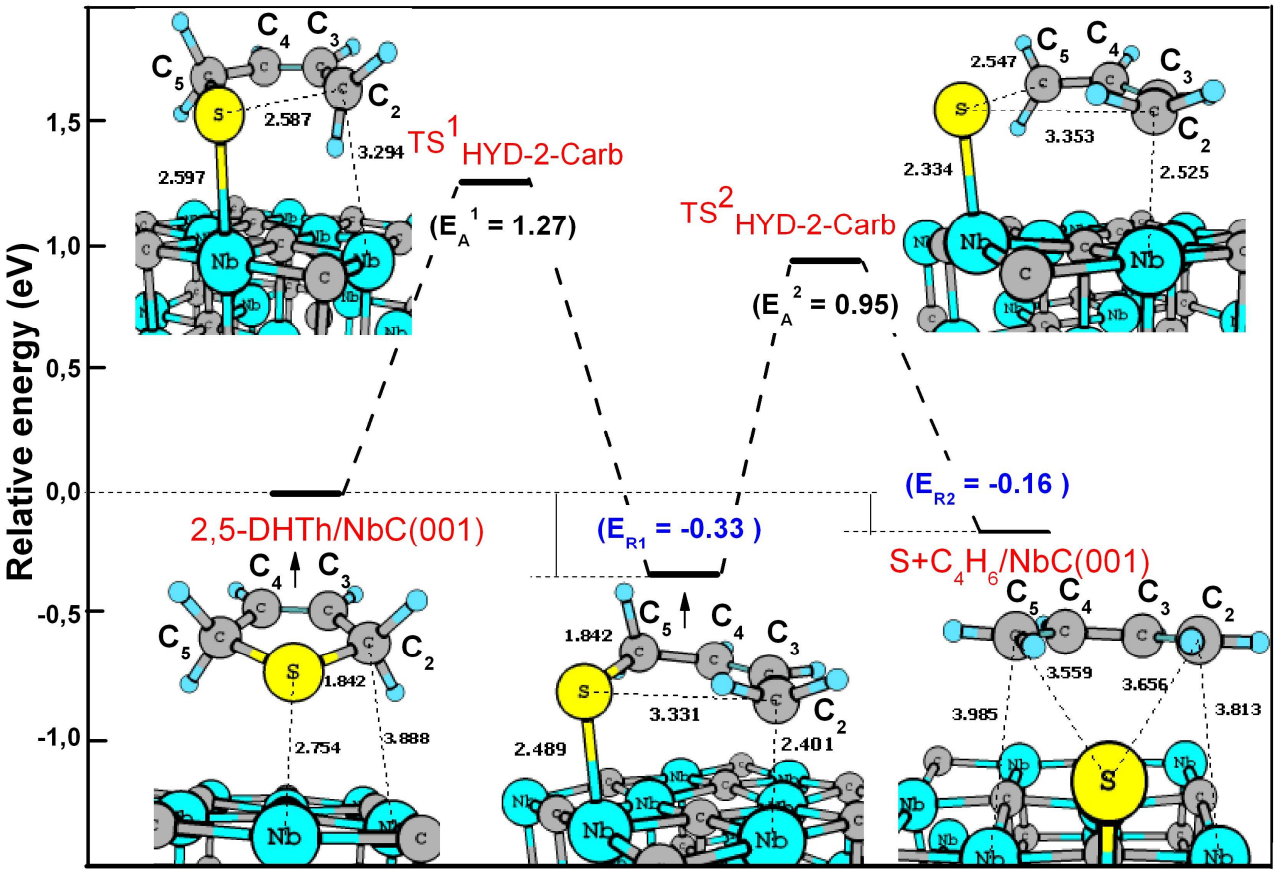

Figure 7

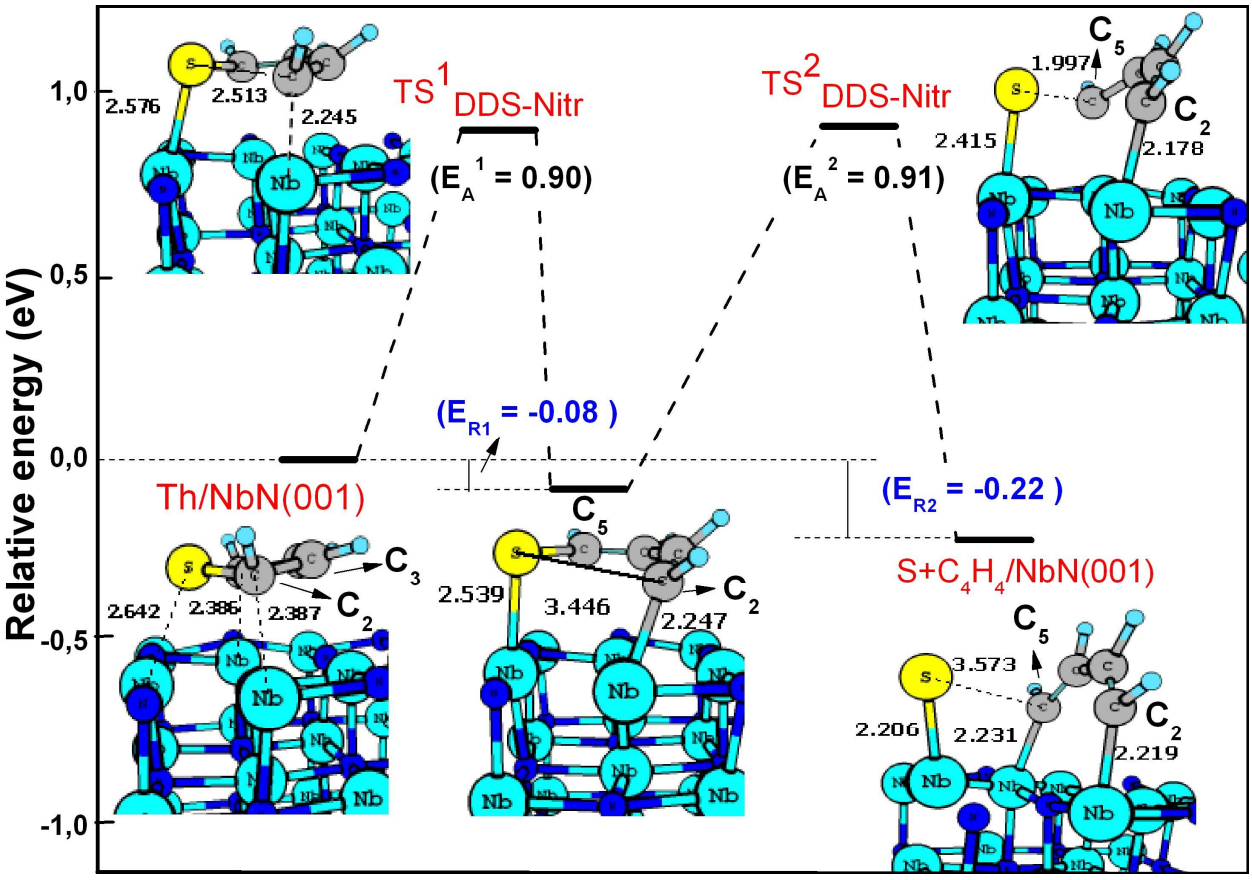

Figure 8

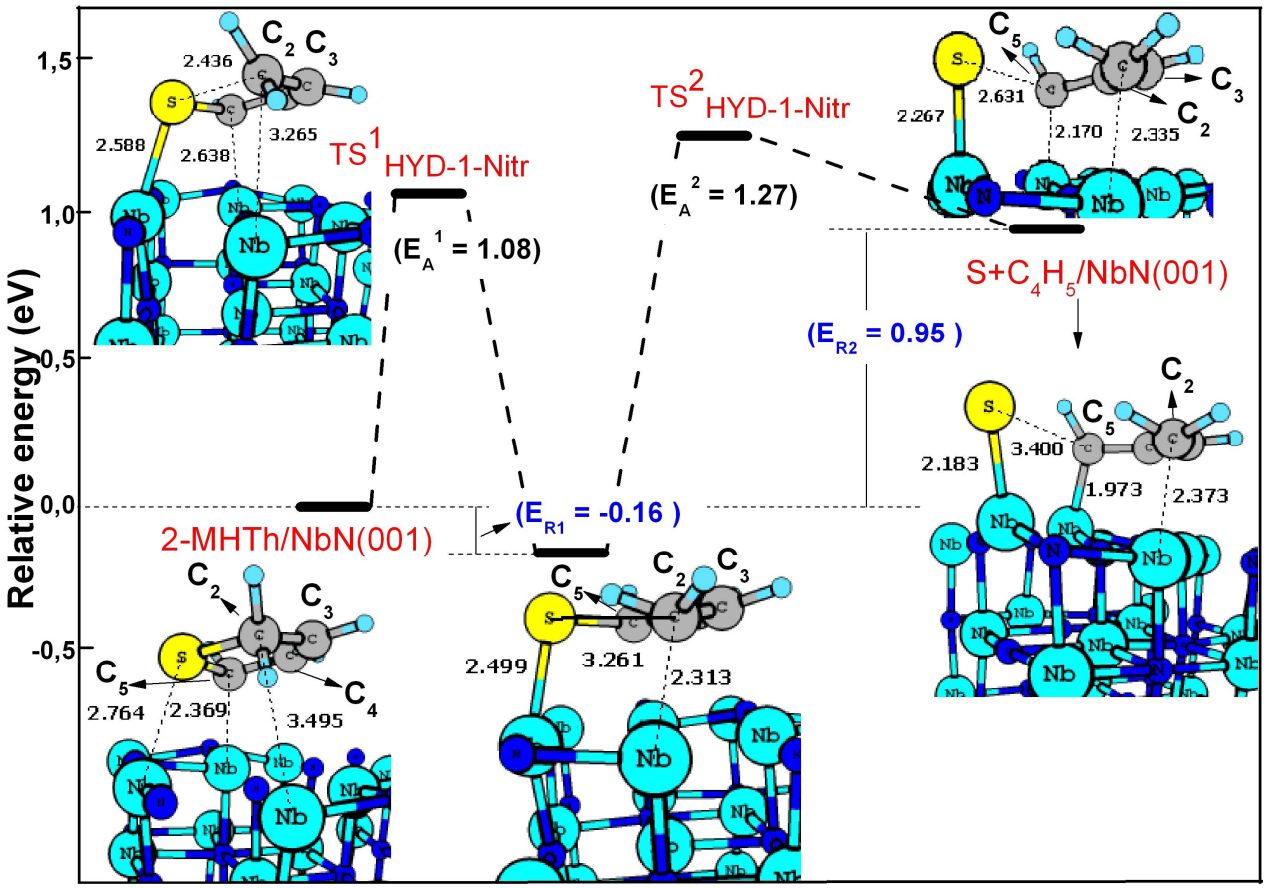

Figure 9

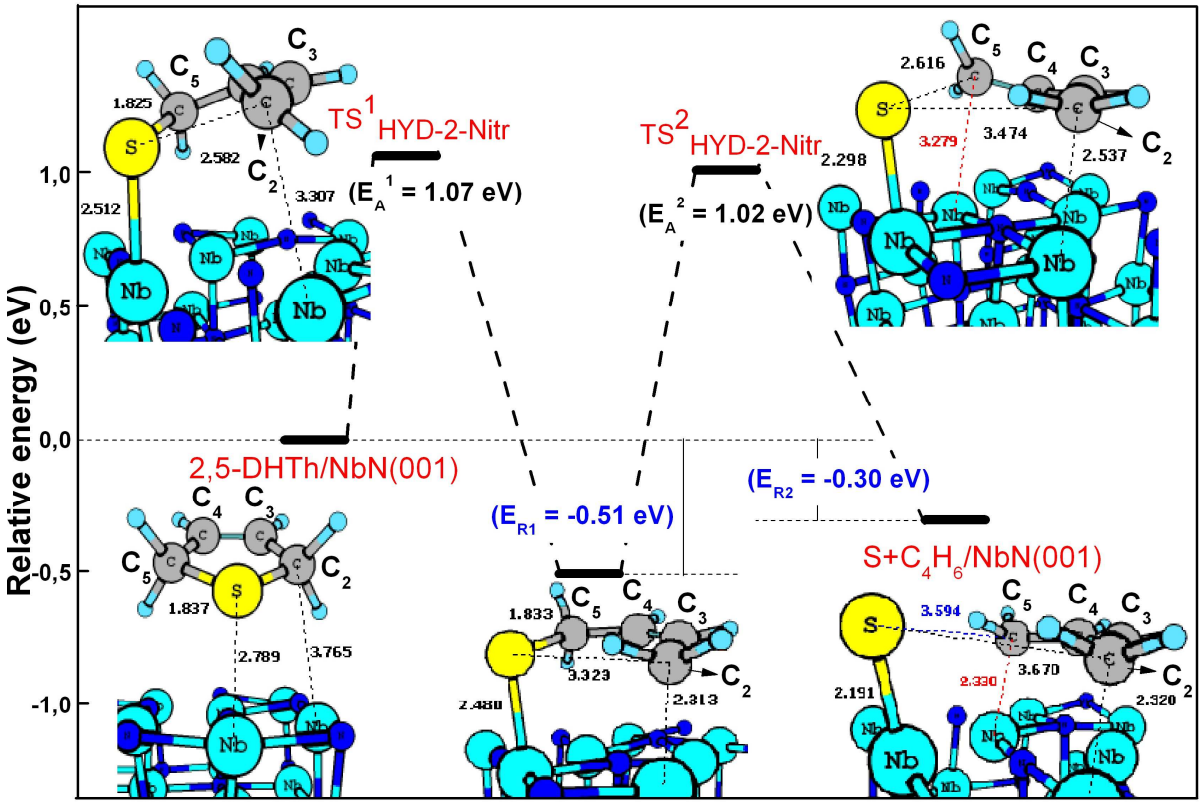

GRAPHICAL ABSTRACT